Hindawi
Journal of Electrical and Computer Engineering
Volume 2022, Article ID 5948356, 18 pages
https://doi.org/10.1155/2022/5948356

Research Article

Design of a Robust Coordinated Power Oscillation Damper for Use with Large-Scale Wind Energy System Connected to a Multimachine Power System

Paul Kabiru,[1] **Keren Kaberere**,[2] **and Stanley Kamau**[2]

[1]*Electrical Engineering Department, Pan African University Institute for Basic Sciences Technology and Innovation, Nairobi, Kenya*
[2]*Electrical and Electronic Engineering Department, Jomo Kenyatta University of Agriculture and Technology, Nairobi, Kenya*

Correspondence should be addressed to Paul Kabiru; paulmkabiru@gmail.com

Received 6 June 2022; Revised 21 September 2022; Accepted 23 September 2022; Published 3 November 2022

Academic Editor: Bhargav Appasani

Many researchers have proposed the use of the doubly fed induction generator (DFIG)-based wind energy conversion system (WECS) in the enhancement of power system dynamic performance. However, the application of a coordinated design strategy to coordinate the DFIG and other synchronous generators in the system for the improvement of small-signal stability is rarely researched. What is more, the use of strategy with a low computational burden to enhance the robustness of coordinated strategy for the design of damping controllers is rare. A coordinated strategy in designing multiple damping controllers, including DFIG-based power oscillation damper (POD) and power system stabilizers (PSSs), is proposed in this paper. A modal participation factor is employed to find out the most effective feedback signal for the POD. A hybrid optimization algorithm based on the grey wolf optimizer (GWO) and particle swarm optimizer (PSO) is applied for parameter optimization of the damping controllers considering a multiobjective eigenvalue-based optimization problem. Modal analysis is carried out on the widely studied two-area four-generator benchmark power system to establish the theoretical viability of the proposed approach. Probabilistic analysis established on Monte Carlo simulation is then carried out to prove the robustness of the coordinated design strategy under diverse operating conditions. Nonlinear time-domain simulations are used to verify the damping performance and robustness of the proposed strategy under different operating scenarios.

1. Introduction

Sustained power oscillations pose a serious problem to the control and operation of power systems. Apart from limiting the capacity of transmission lines, oscillations in the power system have been attributed to safety issues in electrical power equipment. In the most serious instances, sustained and rising power oscillations can cause the eventual collapse of the entire power system if no proper measures are undertaken early enough.

Power system stabilizers (PSS), which are widely equipped in synchronous generators, have been used for damping control and stabilization of power system oscillations [1]. The PSSs have been effective in the provision of damping in the conventional power system which has been dominated by synchronous generators. Modern power systems, however, have increasingly experienced a surge in nonconventional energy sources which might limit the damping performance provided by the PSSs. New measures of damping oscillations need to be established.

Given the current energy crises and environmental issues associated with conventional energy sources, the use of renewable energy, particularly wind energy, has become widespread globally [2]. Doubly fed induction generators (DFIG) are the most common among the variable wind generation systems because of their relatively high efficiency and low costs [3]. Increased proportionate integration of wind energy systems plays a critical role in power system stability [4]. Nevertheless, wind energy integration might enhance power system stability [5]. Previous research has

shown that DFIG-based wind generators can enhance the power system's dynamic stability and, in addition, contribute to network support during faults [6]. Furthermore, the use of auxiliary damping controllers in DFIG-based wind generators to improve damping performance has become a research hotspot [7]. The use of power oscillation damper (POD) to describe damping controllers established in renewable energy systems has become a widely accepted term [8]. The main advantage of the DFIG-based POD is that they are adapted from the classical lead-lag PSS [9]. Therefore, most of the already established methods used in the design of PSS can be applied to design the POD.

The design of a single kind of damping controller is a common engineering practice. However, the coordinated design of damping controllers can enhance the dynamic performance of the power system as well as make the operations of the power system more flexible [7]. When different kinds of damping controllers are present in the power system, how to come up with a coordinated strategy for damping controller design is challenging. This work is devoted to providing an alternative solution to simultaneous and robust coordinated damping control in a multimachine power system comprising a large-scale wind energy system and synchronous generators. The coordinated design strategy allows multiple damping controllers in the power system, including POD and PSS, to be optimized simultaneously, thus ensuring the optimized damping controllers provide robust damping performance under multiple operating conditions of the system. In contrast, the uncoordinated design considers each damping controller optimized separately, mostly at the rated power output of the generator it is integrated into. Since the uncoordinated design does not take into consideration the effect of interactions between the local machine and other machines in the system, it may not provide robust damping control under all the operating points of the power system [10].

Whereas the design of a single kind of damping control has received considerable research focus, there has been less attention on the coordinated strategy for the design of multiple damping controllers, whose need has become common in the present-day power system. A damping controller for wind energy generators designed using evolutionary PSO was observed to improve the damping of electromechanical oscillations over a variety of operating scenarios [11]. In Ref. [12], a damping controller for a DFIG-based wind energy conversion system (WECS) using the slip as the input to modulate the rotor flux in the flux magnitude angle control (FMAC) was found to enhance the damping contribution of the WECS. The use of the firefly algorithm in the design of a robust POD for a decentralized DFIG-based WECS considering system uncertainties modeled using the H_∞/H_2 demonstrated that the DFIG POD can be robust against heavy power flows, wind patterns, fault location, and even severe power faults [13]. The authors [14] show that the use of a damping controller in a DFIG, integrated into a two-area system and utilizing wide-area feedback signals, can achieve a greater damping performance than when the damping controller is used in a similar synchronous generator. While the above literature consider the uncoordinated design of the POD, they also rarely consider large-scale wind farm of equivalent capacity to other synchronous generators in the system. A parameter optimization method using probability theory, and applying the particle swarm optimizer (PSO), demonstrated the robust coordinated design of PSS and POD considering 1000 operating conditions [15]. A coordinated damping control scheme, applying the PSO for the design of damping controllers in DFIG and synchronous generators considering a probabilistic model for wind speed and using extended probabilistic small-signal stability, established the robustness of the DFIG POD under various wind speeds [16]. These methods do not take into account the computational effort required to meet the desired robustness. Surinkaew and Ngamroo [17] demonstrated the robust coordination of two decentralized PODs each installed in a 100 MW DFIG-based WECS added to areas 1 and 2 of the two-area system, using the firefly algorithm. For robustness, the design of the POD considered uncertainties modeled using the inverse output multiplicative model. The improvement in the damping ratio of the critical modes with the coordinated PODs, with respect to when there were no damping controllers, however, was below 12%. This could be attributed to the use of the damping controllers in decentralized DFIGs with less power output (100 MW) with respect to other synchronous generators in the system (700 MW). Zuo et al. [18] demonstrated the coordination of FACTS-based static VAR compensator (SVC) POD, in addition to DFIG POD and PSSs, for a two-area four-generator test system. The 100 MW DFIG-based WECS was integrated into area 1 and the SVC was installed at the middle of the tie line. Whereas the method proved to be computationally efficient and capable of damping electromechanical oscillations, it required a complex wide-area measurement system (WAMS) to transmit the wide-area POD input signal and risked invalidity of the controllers under reversal of tie line power.

A novel robust coordinated strategy for damping control design is proposed in this paper. The method simultaneously designs multiple damping controllers, including PSSs and large-scale wind farm-based PODs, to suppress local and interarea low-frequency oscillations and to improve the system's dynamic performance. The POD for the DFIG-based wind farm is adapted from the classical lead-lag PSS. The modal participation factor is used to determine the most effective DFIG feedback signal for the POD. Modal analysis is also employed to establish the critical low-frequency oscillation modes of the system. To ensure robustness while maintaining a low computation burden, the design strategy employed in this paper takes into account the operating scenarios that have the worst impact on the identified critical oscillation modes for optimization purposes. The recently proposed hybrid optimization algorithm applying grey wolf optimization and particle swarm optimization (GWO-PSO), which has been proven to have superior convergence performance in literature with constrained multimodal problems, as well as high solution quality and stability, is applied for optimization of the damping controller parameters [19].

The rest of this paper is ordered as follows. The mathematical models for the power system including the

excitation system for synchronous generators and the DFIG and the damping controllers present in the system including PSSs and POD are presented in Section 2. The selection of the most suitable wind farm-based feedback signal as the input for the POD, the formulation of the multiobjective eigenvalue-based optimization problem, and the application of the hybrid GWO-PSO for parameter optimization of the damping controllers in the coordinated design strategy are outlined in Section 3. Linear modal analysis without and with the coordinated strategy for damping controller design in the critical operating scenarios, an analysis of robustness based on probabilistic Monte Carlo simulation, and verification of the performance of the coordinated design strategy using nonlinear time-domain simulations are then demonstrated in Section 4. The conclusions of the findings are finally presented in Section 5.

2. Mathematical Modeling

2.1. Model of AVR including PSS for Synchronous Generators. An AVR forms the basis of voltage regulation in a synchronous generator. It measures the terminal voltage and compares it with the reference voltage, and the error is used to adjust the field voltage through, generally, proportional control [20]. Although the dynamic model of AVR comprises several parameters, the AVR gain and feedback delay time constant can accurately model the small-signal dynamics of AVR. The PSS introduces an electrical torque that varies with rotor speed variations (damping torque). While the damping contribution of the PSS is largely determined by the PSS gain, a washout filter time constant and washout gain enables the PSS to filter unnecessary steady-state components from the input, whereas the time constants for the lead-lag stage determine the phase compensation for the PSS output signal.

The block diagram of the AVR and PSS is depicted in Figure 1.

The AVR dynamic behavior is given by

$$E_{\text{fd}} = K_A\left(V_{\text{ref}} + V_{\text{pss}} - v\right), \tag{1}$$

where V_{ref} and E_{fd} constitute the voltage set point and the output voltage of the AVR, respectively; V_{PSS} is the auxiliary stabilization signal from the PSS; and v is the principal AVR input signal from the synchronous generator voltage transducer. The constants K_A and T_R in Figure 1 represent the AVR gain and feedback delay time constant, respectively, while $E_{\text{fd}}^{\max}$ and $E_{\text{fd}}^{\min}$ define the limits of the output of the excitation system imposed by the overexcitation and underexcitation limiter, respectively [21].

The common lead-lag PSS shown in Figure 1 is used in this study. The PSS modulates the principal input signal of the excitation system by introducing a purely damping torque. As a result, it increases the damping torque of the synchronous generator and suppresses rotor oscillations between the synchronous generators [21]. The dynamic behavior of the PSS is defined using

$$V_{\text{pss}} = K_{\text{STAB}}\frac{sT_W\left(1+sT_1\right)\left(1+sT_3\right)}{\left(1+sT_W\right)\left(1+sT_2\right)\left(1+sT_4\right)}\Delta\omega, \tag{2}$$

where V_{pss} is the PSS output signal, $\Delta\omega$ is the speed deviation in rad/s which acts as the input of the PSS, K_{STAB} is the PSS gain, T_W is the time constant for the washout filter, usually selected as 10 s, and T_1, T_2, T_3, and T_4 are the time constants in seconds for the two lead-lag compensators of the PSS [21].

2.2. Model for DFIG-Based Windfarm including POD. DFIG wind farm comprises many modular wind turbines which are connected in parallel. Since this study focuses on the electromechanical behavior of the system, the wind turbine dynamic model depicted in Figure 2 is chosen. In the model, the mechanics of the wind turbine including the pitch control and speed control are modeled. In addition, the electrical control of the rotor side converter (RSC), including the current control, and active and reactive power control, is modeled.

The dynamic equations of the DFIG oriented in the synchronous speed rotating reference frame, the *d-q* reference frame, are given in actual SI units as follows [22]:

$$\begin{bmatrix} v_{ds} \\ v_{qs} \end{bmatrix} = -R_s\begin{bmatrix} i_{ds} \\ i_{qs} \end{bmatrix} + \frac{d}{\text{dt}}\begin{bmatrix} \psi_{ds} \\ \psi_{qs} \end{bmatrix} + w_s\begin{bmatrix} -\psi_{qs} \\ \psi_{ds} \end{bmatrix},$$
$$\begin{bmatrix} v_{dr} \\ v_{qr} \end{bmatrix} = -R_r\begin{bmatrix} i_{dr} \\ i_{qr} \end{bmatrix} + \frac{d}{\text{dt}}\begin{bmatrix} \psi_{dr} \\ \psi_{qr} \end{bmatrix} + \left(w_s - w_r\right). \tag{3}$$

The stator and rotor fluxes are given as

$$\begin{bmatrix} \psi_{ds} \\ \psi_{qs} \end{bmatrix} = -\begin{bmatrix} X_s i_{ds} + X_m i_{dr} \\ X_s i_{qs} + X_m i_{qr} \end{bmatrix},$$
$$\begin{bmatrix} \psi_{dr} \\ \psi_{qr} \end{bmatrix} = -\begin{bmatrix} X_r i_{dr} + X_m i_{ds} \\ X_r i_{qr} + X_m i_{qs} \end{bmatrix}, \tag{4}$$

where the stator voltage and current are given by $v_{dqs} = v_{ds} + jv_{qs}$ and $i_{dqs} = i_{ds} + ji_{qs}$, respectively; the rotor voltage and current are given by $v_{dqr} = v_{dr} + jv_{qr}$ and $i_{dqr} = i_{dr} + ji_{qr}$, respectively; the stator and rotor fluxes are given by $\psi_{dqs} = \psi_{ds} + j\psi_{qs}$ and $\psi_{dqr} = \psi_{dr} + j\psi_{qr}$, respectively; the stator and rotor reactance are given by $X_s = X_{ls} + X_m$ and $X_r = X_{lr} + X_m$, respectively, where X_{ls} and X_{lr} are the leakage reactance of the stator and the rotor, and X_m is the magnetizing reactance; R_s and R_r are the stator and rotor resistance, respectively; and w_s and w_r are the synchronous and rotor speed of the DFIG, respectively.

The stator *d-q* voltage components are derived from the DFIG output voltage, v, as follows:

$$v_{ds} = -v\sin\theta,$$
$$v_{qs} = v\cos\theta. \tag{5}$$

The active power and reactive power output of the DFIG comprise the sums of power from the stator and that from the converter and are described as follows [18]:

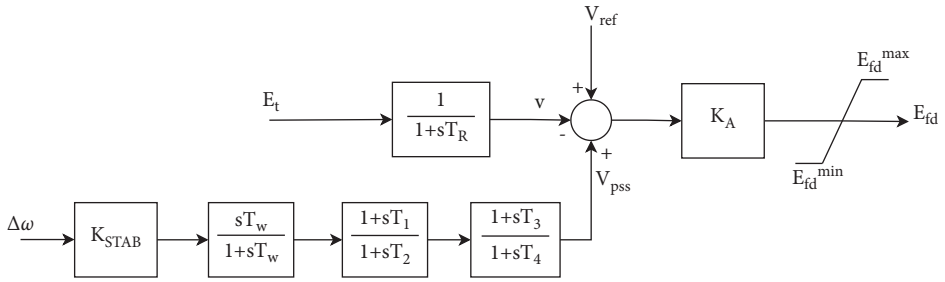

Figure 1: Block diagram of the excitation system and PSS.

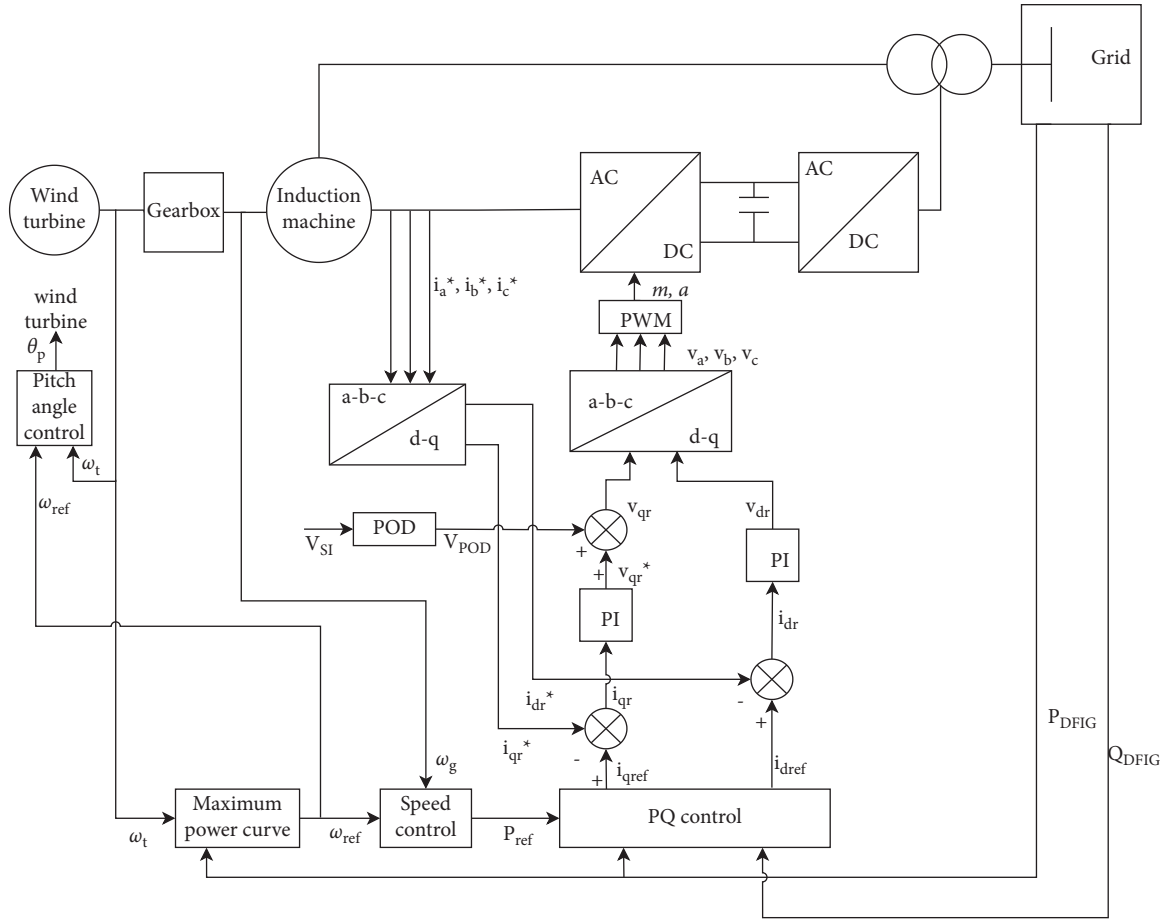

Figure 2: Schematic of the doubly fed induction generator (DFIG) model and its controls.

$$P_{\mathrm{DFIG}} = v_{ds}i_{ds} + v_{qs}i_{qs} + v_{dc}i_{dc} + v_{qc}i_{qc},$$
$$Q_{\mathrm{DFIG}} = v_{qs}i_{ds} - v_{ds}i_{qs} + v_{qc}i_{dc} - v_{dc}i_{qc}, \tag{6}$$

where i_{dc}, i_{qc}, v_{dc}, v_{qc} symbolize the converter currents and voltages, respectively, in the d-q reference frame.

The converter power on the grid side converter is given as follows:

$$P_c = v_{dc}i_{dc} + v_{qc}i_{qc},$$
$$Q_c = v_{qc}i_{dc} - v_{dc}i_{qc}. \tag{7}$$

Similarly, the converter active and reactive powers on the rotor side are equal to the respective rotor powers and are given as follows:

$$P_r = v_{dr}i_{dr} + v_{qr}i_{qr},$$
$$Q_r = v_{qr}i_{dr} - v_{dr}i_{qr}. \tag{8}$$

Assuming an ideal converter, $P_r = P_c$, the DFIG injects electrical power into the grid which is expressed as follows:

$$P_{\mathrm{DFIG}} = v_{ds}i_{ds} + v_{qs}i_{qs} + v_{dr}i_{dr} + v_{qr}i_{qr},$$
$$Q_{\mathrm{DFIG}} = v_{qs}i_{ds} - v_{ds}i_{qs} + v_{qr}i_{dr} - v_{dr}i_{qr}. \quad (9)$$

In addition to the electrical model, a DFIG is also described by the mechanical model which relates aerodynamic torque to the electrical torque through the shaft dynamics [16]. The shaft dynamics are represented by a two-mass model, with the dynamics of generator inertia and rotor inertia being modeled separately. The turbine inertia dynamics are modeled as follows where the variables are in actual SI units:

$$J_t\frac{dw_t}{d\mathrm{t}} = T_a - T_{ls},$$
$$T_a = \frac{1}{2}\rho\pi R^2\frac{C_p(\lambda,\beta)}{\lambda}v^2, \quad (10)$$
$$T_{ls} = K_{ls}(\theta_t - \theta_{ls}) + B_{ls}(w_t - w_{ls}),$$

where J_t is the turbine inertia, w_t and w_{ls} are the rotor mechanical speed and the low-speed shaft speed, respectively, T_a and T_{ls} represent the aerodynamic torque and the low-speed shaft torque at the gearbox, respectively. $C_p(\lambda,\beta)$ is the dimensionless aerodynamic power coefficient, ρ symbolizes the air density, v is the wind velocity, R is the blade radius, β represents the blade angle, while the tip speed ratio is given by λ. K_{ls} represents the low-speed shaft stiffness; θ_t and θ_{ls} are the positions of the turbine and the low-speed shaft at the gearbox, respectively.

The generator inertia dynamics are described as follows:

$$J_g\frac{dw_g}{d\mathrm{t}} = T_{hs} - T_e,$$
$$T_{hs} = n_g T_{ls},$$
$$T_e = \psi_{qr}i_{dr} - \psi_{dr}i_{qr} = \psi_{ds}i_{qs} - \psi_{qs}i_{ds} = X_m\left(i_{qr}i_{ds} - i_{dr}i_{qs}\right), \quad (11)$$

where J_g is the inertia of the generator, w_g is the generator speed, T_{hs} is high-speed shaft torque assuming an ideal gearbox, n_g is the gearbox ratio, and T_e is the generator's electromagnetic torque.

The detailed dynamic models for the DFIG control subsystems, including pitch control, speed control, and active and reactive power control, can be found in the DigSILENT PowerFactory technical manual [23]. The DFIG is provisioned with a POD which modulates the voltage of the rotor in the active power control loop, thus providing supplementary damping for electromechanical oscillations. The structure of the POD is based on that of the classical PSS of the synchronous generator. Figure 3 shows the block diagram of the DFIG POD.

The POD comprises a stabilizer gain K_{POD} which majorly determines the supplementary damping provided by the POD, a washout stage with a time constant T_W that eliminates unnecessary steady-state components from the POD input, and a 2nd order lead-lag compensator constituting the time constants T_1, T_2, T_3, T_4 which provides phase compensation for the damping signal. The input to the POD is the speed deviation which is the difference between the speed of the turbine and that of the generator. An antiwindup limiter is present which limits the POD output, V_{POD}, to within ±0.1 pu . The antiwindup limiter prevents excessive signal magnitudes from the POD from compromising the proper operation of the DFIG that the POD is integrated into.

The feedback signal V_{SI}, which acts as the input to the POD, as well as the DFIG control signals the POD output is added to, both play a critical role in the effectiveness of the POD. The POD comprises a controller that adds a modulated signal to the rotor voltage, which corresponds to the output of the rotor side converter. Previous literature has shown that the damping signal from the POD can be added to the quadrature rotor voltage, V_{qr}^*, in the active power control loop, or to the direct rotor voltage, V_{dr}, in the reactive power control loop of the DFIG [11]. In this study, the output signal of the POD, V_{POD}, is added to the quadrature rotor voltage in the active power control loop, as shown in Figure 2. It has been established that when the signal is added to this loop, it provides better damping performance than when it is added to the reactive power control loop [14]. Furthermore, reactive power modulation has the disadvantage of introducing oscillations in the terminal voltage profile of the DFIG [24]. Through modulation of active power, the POD provides a damping torque that is in phase with the rotor speed deviation, similar to PSS and FACTS devices used for the same purpose. The selection of suitable feedback signals for the POD is elaborated in Section 3.1.

2.3. Dynamic Model for the Power System. The behavior of a dynamic multimachine power system is modeled using differential and algebraic equations as follows:

$$\dot{x} = f(x,u),$$
$$y = g(x,u), \quad (12)$$

where $f(x,u)$ is a system of differential-algebraic equations describing the dynamic components and nonlinear components, and $g(x,u)$ is a system of output equations. The equations are functions of the state variable x, and the input variables u, considering a time-invariant system.

The dynamic algebraic equations of the system after it is perturbed become

$$x. = f(x_0 + \Delta x, u_0 + \Delta u),$$
$$y = g(x_0 + \Delta x, u_0 + \Delta u), \quad (13)$$

where Δu and Δx are the perturbations on the input variable and the state variable, respectively. After linearizing all the components of x and y vectors of the perturbed system around the specified operating state, the following set of equations is obtained

$$\Delta\dot{x} = A\Delta x + B\Delta u,$$
$$\Delta y = C\Delta x + D\Delta u, \quad (14)$$

where A, B, C, D symbolize the state, input, output, and feedforward matrices of the state-space model, respectively.

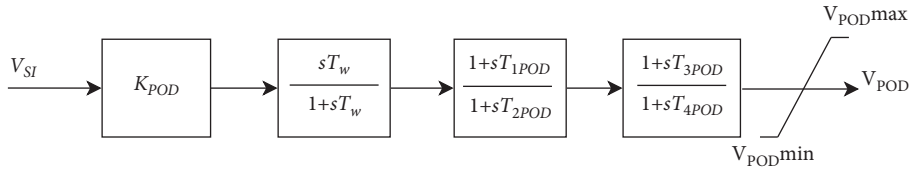

Figure 3: Block diagram for the DFIG power oscillation damper (POD).

Equation (14) is the model, in the state-space form, of a multimachine power system and is used when performing modal analysis and designing damping controllers for the power system. The system eigenvalues, derived from state matrix A, divulge the system's asymptotic stability at the equilibrium point. The eigenvalues, λ, are computed by solving

$$\det(A - \lambda I) = 0. \tag{15}$$

The damping is determined by the real part of the eigenvalue whereas the imaginary part determines the oscillation frequency as shown in (16). Complex eigenvalues normally exist in pairs, and they are related to an oscillatory mode. A real eigenvalue is related to an aperiodic/non-oscillatory mode. When an eigenvalue is real and negative, the aperiodic mode decays proportional to the magnitude of the eigenvalue whereas a real positive eigenvalue signals aperiodic instability.

$$\lambda = \sigma \pm j\omega. \tag{16}$$

For each eigenvalue, there is a right and left eigenvector. The right eigenvector defines the absolute activity of state variables in a given oscillation mode while the relative contribution of the state variable activity to the given mode is described by the left eigenvector. Participation factors combine the left and right eigenvectors and measure the association between the modes and the state variables. State variables that have the highest participation in a given mode are likely to influence the small-signal stability of the mode. The participation factor is used to select the most suitable feedback signal for the POD in Section 3.1.

The damping ratio is used to characterize how oscillations in the system decay after a disturbance. It describes how rapidly oscillations decay relative to the frequency of oscillations and is given by

$$\zeta = \frac{-\sigma}{\sqrt{\sigma^2 + \omega^2}}. \tag{17}$$

The damping ratio is usually expressed as a percentage. Unstable electromechanical modes have a damping ratio of less than 0% while stable electromechanical modes have a damping ratio greater than 0%.Stable aperiodic modes have a damping ratio of 100% whereas stable oscillatory modes have a damping ratio of less than 100% but greater than 0%. Although there is not a universally acceptable value of damping ratio to describe adequately damped oscillation modes, a damping ratio of 20% can provide a sufficient margin of stability [18]. Oscillation modes with a damping ratio below this threshold are referred to as poorly/lightly damped modes. The damping ratio is used to formulate the objective function for the optimization problem in Section 3.2.

3. Design of Robust Coordinated Damping Control

3.1. Selection of Input Signals for the DFIG POD. The consideration of suitable feedback signals for the POD is a significant factor in designing an effective damping controller as well as the coordination of several supplementary damping controllers. An effective damping controller ensures the local electromechanical oscillations, due to interaction between many DFIG units in the wind farm, are effectively damped. By principle, the feedback signal selected should greatly influence the electromechanical modes of interest while having little to no impact on other unconcerning modes [18]. Although global feedback signals, such as the tie line active power, are the most suitable for suppression of global modes of oscillation in the power system, these feedback signals require complex wide-area measurement systems (WAMS). For instance, the GPS-based WAMS, comprising phasor measurement units (PMUs) and phasor data concentrators (PDCs), is ideally considered for monitoring and control of progressively sophisticated behavior shown by the electrical power system [25].

Suitable local feedback signals to the DFIG POD can guarantee electromechanical oscillation modes in the wind farm are sufficiently damped. Furthermore, coordination of the POD with other PSSs in the system can ensure not only local wind farm modes but also the global oscillation modes which are adequately damped. In this study, the modal participation index is used to determine the most suitable local feedback signal for the POD. The participation factor acts as a measure of the correlation between the modes of oscillation and the state variables [7]. It accounts for the joint modal controllability and observability of the feedback signal in the concerning modes. The feedback signal should be both controllable and observable. The participation factor of the k^{th} state variable in relation to the i^{th} mode is expressed as follows:

$$p_{ik} = v_{ik}u_{ki}, \tag{18}$$

where v_{ik} is the element on the k^{th} column and i^{th} row of the modal controllability matrix V, while u_{ki} is the element on the i^{th} column and k^{th} row of the modal observability matrix U. The modal controllability matrix, which is based on the

left eigenvector, describes the contribution of the activity of state variables to the mode and is derived as follows:

$$\begin{aligned} v_i A &= \lambda_i v_i, \\ v_i &= \left[v_{i1} \dots v_{ik} \dots v_{\text{in}}\right], \\ V &= \left[v_1^T \dots v_i^T \dots v_n^T\right]. \end{aligned} \tag{19}$$

Similarly, the modal observability matrix, which is based on the right eigenvector, describes the behavior of state variables in the mode and is derived as follows:

$$\begin{aligned} A u_i &= \lambda_i u_i, \\ u_i &= \left[u_{i1}^T \dots u_{ik}^T \dots u_{\text{in}}^T\right], \\ U &= \left[u_1 \dots u_i \dots u_n\right]. \end{aligned} \tag{20}$$

3.2. Optimization Problem Formulation. The key objective of a coordinated strategy in designing several damping controllers is to improve the overall power system performance in damping electromechanical oscillations. To optimize the damping capability of the damping controllers, a multi-objective eigenvalue approach is considered for this study [26]. The objective function is given as

$$\text{Minimize } J = \sum_{j=1}^{\text{no}} \sum_{\zeta_{i,j} < \zeta_0} \left(\sigma_0 - \sigma_{i,j}\right)^2 + \left(\zeta_0 - \zeta_{i,j}\right)^2, \tag{21}$$

where no represents the number of operating scenarios considered in the tuning of parameters for POD and PSSs. $\zeta_{i,j}$ denotes the damping ratio of the ith mode of oscillation in the jth operating scenario, ζ_0 represents the minimum desired damping ratio, σ_0 is the desired maximum real part of the eigenvalues, while $\sigma_{i,j}$ denotes the real part of the ith damping ratio in the jth operating scenario. Only the modes with a damping ratio $\zeta_{i,j} < \zeta_0$ are considered in the optimization process. The minimization of objective function J will therefore place the eigenvalues to the desired sector on the left side of the s-plane where the damping ratio $\zeta_{i,j} \geq \zeta_0$ and eigenvalues real part $\sigma_{i,j} \leq \sigma_0$, as shown in Figure 4.

The constraints for the optimization problem represent the lowest and highest bounds for the parameters of the damping controllers optimized utilizing the proposed method. The optimized parameters comprise the POD and PSS gains K_{POD} and K_{STAB}, respectively, and time constants for the 2nd order lead-lag compensator of the PSS and POD, T_1, T_2, T_3 and T_4.

The optimization problem is therefore expressed as minimization of J subject to

$$\begin{aligned} K_{\text{STAB}}^{\min} &\leq K_{\text{STAB}} \leq K_{\text{STAB}}^{\max}, \\ K_{\text{POD}}^{\min} &\leq K_{\text{POD}} \leq K_{\text{POD}}^{\max}, \\ T_{1,2,3,4}^{\min} &\leq T_{1,2,3,4} \leq T_{1,2,3,4}^{\max}. \end{aligned} \tag{22}$$

The lower limits and upper limits considered are [0.1 50] for K_{STAB}, [0.1 1] for K_{POD}, and [0.1 1] for T_1, T_2, T_3, and T_4 . These limits are considered in most literature to ensure the desired operation without making the exciter mode unstable

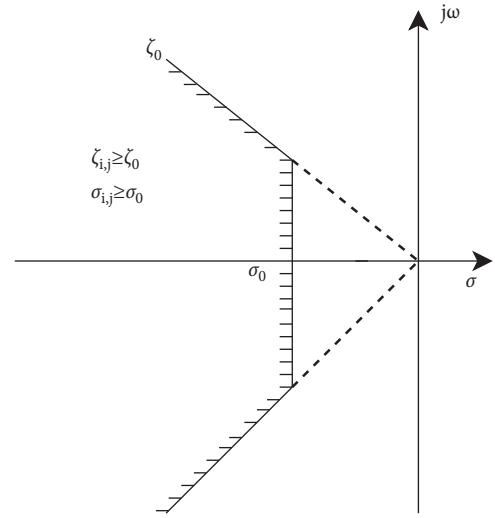

Figure 4: Desired region for the eigenvalues on the s-plane.

[18]. The washout time constant is chosen as 10 s which is, in practice, generally sufficient to eliminate the unnecessary steady-state components from the input of the damping controller [21].

3.3. Application of the Hybrid GWO-PSO Algorithm. In 2014, Mirjalili et al. [27] presented a novel swarm intelligence method acknowledged by the name grey wolf optimizer (GWO), which is encouraged by the hunting mechanism and leadership hierarchy of the grey wolves. On the other hand, the PSO is among the most applied bio-inspired techniques in hybrid variants because of its ability to search the global optimum, simplicity, and speed of convergence [28]. It is a population-based optimization technique. It is inspired by the collective social behavior of animals that interact with each other in swarms, such as the flocking of birds or schooling of fish, in search of food. The technique of PSO was first invented by Kennedy and Eberhart in 1995 [29]. Both GWO and PSO have shown promising performance over most swarm intelligence metaheuristics in literature. In Ref. [30], the GWO was used for the optimization of reactive power where it is proved to be superior to other algorithms such as imperialist competitive algorithm (ICA), gravitational search algorithm (GSA), harmony search algorithm (HSA), invasive weed optimization (IWO), simple genetic algorithm (SGA), PSO, and comprehensive learning PSO (CLPSO). A comparative study among different nature-inspired algorithms, including cuckoo search (CS), genetic algorithm (GA), PSO, artificial bee colony (ABC), firefly algorithm (FFA), and GWO, regarding the optimization of different benchmark functions, established the promising convergence performance of PSO while the GWO achieved the best overall fitness [31, 32].

Grey wolves are members of the Canidae family and are apex predators. Their population is organized into four diverse clusters: alpha, beta, omega, and delta wolves. There is a male and a female leader both referred to as the alphas who make decisions such as sleeping, waking, and hunting. The second group, the betas, is subordinate to the alphas in

making decisions and ordering the omegas. The omegas play the role of scapegoat and submit to all dominant wolves. The deltas are not part of the alpha or beta but they dominate the omega. To perform optimization, hunting in the GWO is broken down into prey searching, encircling, and attacking. Searching the prey symbolizes the exploration ability of GWO whereas attacking it signifies its exploitation ability. The general encircling behavior of each agent in the population is expressed in the form:

$$\begin{aligned}\vec{D} &= \left|\vec{C} \cdot \vec{X_p}(t) - \vec{X}(t)\right|,\\ \vec{X}(t+1) &= \vec{X_p}(t) - \vec{A} \cdot \vec{D},\end{aligned} \tag{23}$$

where $\vec{D}$ is the current distance of each grey wolf from the prey, $\vec{X}(t)$ represents the current wolf position, $\vec{X_p}(t)$ indicates the prey position, $\vec{C}$ and $\vec{A}$ are coefficient vectors based on random numbers that make the prey evade the wolf and adjust the position of the grey wolves to make them reach different places around the best search agents, respectively. The coefficient vectors are given by

$$\begin{aligned}\vec{A} &= 2.\vec{a} \cdot \vec{r_1} - \vec{a},\\ \vec{C} &= 2 \cdot \vec{r_2},\end{aligned} \tag{24}$$

where $\vec{a}$ is a value that linearly decreases from 2 to 0 during iteration; $\vec{r_1}$ and $\vec{r_2}$ are random vectors in the space [0, 1]. While searching for the prey, the random value A is considered in space $[-2, 2]$. If $|A| < 1$, the wolves will attack the prey; else, they retrieve. The governing equations for the first three agents (alphas, beta, and delta) are as follows:

$$\begin{aligned}\vec{D_\alpha} &= \left|\vec{C_1} \cdot \vec{X_\alpha} - \vec{X}\right|,\\ \vec{D_\beta} &= \left|\vec{C_2} \cdot \vec{X_\beta} - \vec{X}\right|,\\ \vec{D_\delta} &= \left|\vec{C_3} \cdot \vec{X_\delta} - \vec{X}\right|,\end{aligned} \tag{25}$$

where the vectors denoting the position of the alpha, the beta, and the omega wolves are given by $\vec{X_\alpha}$, $\vec{X_\beta}$, and $\vec{X_\delta}$, respectively, while $\vec{X}$ indicates the position vectors of the current wolf. The omegas are guided by the first three agents in encircling the prey.

The current individual position of the wolves relative to the alpha, beta, and delta wolf, respectively, is given by

$$\begin{aligned}\vec{X_1} &= \vec{X_\alpha} - A \cdot \vec{D_\alpha},\\ \vec{X_2} &= \vec{X_\beta} - A \cdot \vec{D_\beta},\\ \vec{X_3} &= \vec{X_\delta} - A \cdot \vec{D_\delta}.\end{aligned} \tag{26}$$

The final positions of the current individual are determined by their positions from the alpha, beta, and delta wolves:

$$X_i^{t+1} = \frac{X_1^t + X_2^t + X_3^t}{3}. \tag{27}$$

An example of swarm intelligence is birds flying together in search of food, where they use their strengths and knowledge, as well as the knowledge of the other birds, to adjust their velocities and positions until they localize where their food is. For PSO, similarly, the particles represent the iterative solutions whose velocities and positions change according to mathematical equations as follows:

$$\begin{aligned}V_i^{t+1} &= \omega V_i^t + c_1 r_1\left(p_i^t - X_i^t\right) + c_2 r_2\left(g^t - X_i^t\right),\\ X_i^{t+1} &= X_i^t + V_i^{t+1},\end{aligned} \tag{28}$$

where ω is a coefficient known as inertia constant; c_1 and c_2 are the acceleration coefficients of the cognitive term and the social term, respectively; t is the number of iterations; i is the particle index in the population; p_i^t is the best position of the ith particle while g^t is the global best position.

The hybrid GWO-PSO optimization method is a recently established optimization technique [19]. While the PSO has a lot of merits including its ability to search the global maxima and robustness to parameter variations, there are chances of it being trapped in the local minima when a heavily constrained problem is involved. Nevertheless, the PSO is still among the most popular nature-inspired algorithms, and due to its easy implementation, it is also the most prominent in hybrid variants. On the other hand, the GWO, which is a recently introduced algorithm, has shown superior performance to most nature-inspired metaheuristics due to its superior search capability. What is more, the hybridization of GWO and PSO has yielded promising results. A hybrid PSO-GWO algorithm significantly outperformed both PSO and GWO not only in the convergence speed and ability to search the global optimum but also in the quality and stability of solutions when the variants were tested against different benchmark functions, including unimodal, multimodal functions, and fixed-dimension multimodal functions [28, 30]. This study considers a hybrid GWO-PSO algorithm based on a low-level coevolutionary technique where the functionalities of both variants are merged and the two variants operate sequentially [28]. Therefore, the exploitation ability of PSO is improved with the exploration capacity of GWO. Although the verification of the performance of GWO-PSO is not in the scope of this work, its proven superior performance with constrained functions as well as the quality and stability of solutions makes it a great candidate for the robust coordinated strategy in the design of multiple damping controllers that is proposed in this paper.

In the hybrid GWO-PSO, the current positions of the entire population are updated using the PSO, unlike in the GWO where they are updated using (27). The velocities of the wolves in the next iteration are determined by

$$V_i^{t+1} = w\left\{V_i^t + c_1 r_1\left(\overrightarrow{X_1} - X_i^t\right) + c_2 r_2\left(\overrightarrow{X_2} - X_i^t\right) + c_3 r_3\left(\overrightarrow{X_3} - X_i^t\right)\right\}, \tag{29}$$

where w is the inertia component; c_1, c_2, c_3 are the acceleration coefficients relative to the alpha, beta, and delta wolves, respectively; r_1, r_2, r_3 are random numbers; and X_i^t is the current wolf position in the population. The updated position of the current wolf in the next iteration is also determined based on the PSO as follows:

$$X_i^{t+1} = X_i^k + V_i^{t+1}. \tag{30}$$

The pseudocode for the hybrid GWO-PSO is as follows (Algorithm 1):

4. Case Study: Two-Area Four-Generator Test System

To demonstrate the theoretical viability of the coordinated strategy in the design of multiple damping controllers, the comprehensive two-area four-generator (2A4G) test system with a weak tie line connecting the two areas is applied [33]. In the test system, one of the synchronous generators is completely substituted with a DFIG wind farm of equal capacity. To demonstrate the suitability of the design approach for the multiple damping controllers, four principal controller cases are adopted. Firstly, eigenvalue analysis is carried out considering the generators in the system without damping controllers. The modes of interest are identified. Secondly, eigenvalue analysis is carried out with all three synchronous generators equipped with PSSs at default settings according to Ref. [21]. Thirdly, the POD is designed while the parameters of the PSSs are maintained at their original settings. The capability of the POD in damping electromechanical modes is demonstrated. Lastly, the design of the POD is coordinated with other PSSs in the system. The superiority of the coordinated damping approach is not just seen in the damping of local oscillation modes but also in damping of interarea mode.

The coordinated strategy for the design of multiple damping controllers is implemented in MATLAB 2017a and DIgSILENT PowerFactory 2021. The parameter optimization of the damping controllers is achieved through peer-to-peer communication between MATLAB and PowerFactory through an implemented communication interface.

4.1. Test System. The test system, founded on the classical near-symmetric two-area system with a weak tie line, is principally used in the study of small-signal analysis and the design of damping controllers. Figure 5 depicts the single-line diagram of the test system.

The synchronous generators in the system are modeled using the 6^{th} order dynamic model, and each generator is equipped with an excitor and classical PSS presented in Figure 1. $G1$ in the benchmark system [21] is substituted with a 700 MW DFIG wind farm (350 DFIGs of 2 MW each) as shown in Figure 5. Generator $G3$ is taken to be the reference machine. The inherent dynamic behavior of the load is modeled with active power having constant current behavior and reactive power having constant impedance behavior. The system data are given in Table 1.

To investigate the damping performance of the proposed optimized multiple controllers' strategy, simulations were run for the following controller cases:

(i) No PSSs or POD

(ii) PSSs with classical settings and no POD

(iii) PSSs with classical settings and POD optimized for damping of DFIG modes

(iv) POD coordinated with PSSs for enhancement of local and interarea oscillation modes damping

In carrying out the modal analysis, three critical modes (with a damping ratio below 20%) in the system are identified. The three modes comprise a local mode at the wind farm ($M1$), a local mode in area 2 ($M2$), and an interarea mode ($M3$).

To achieve robustness in the coordinated strategy, three principal power flow scenarios are taken into consideration while undertaking the eigenvalue analysis for each of the controller cases mentioned above. The principle operating scenarios are established by running trial power flow studies and observing the resultant impacts on each of the above critical modes. Based on the observations, inferences are made on elements whose loading significantly affects the critical modes. It is observed that the DFIG mode is significantly affected by the DFIG loading. The local mode in Area 2 is significantly affected by the loading of the generators in Area 2. The interarea mode is largely affected by the loading of the tie line. Each of the principle operating scenarios is then chosen such that it results in the poorest damping ratio of one of the three critical modes mentioned above, considering power flow constraints. The scenarios can therefore be referred to as the critical operating scenarios. Table 2 outlines the variances between the critical operating scenarios, while the rest of the elements in the system retain the nominal ratings in the benchmark two-area system [21].

Operating scenarios 1, 2, and 3 results in the poorest damping for the critical modes $M2$, $M1$, and $M3$, respectively, without accounting for outage contingencies.

4.2. Modal Analysis without Damping Controllers. The results in Table 3 show the damping ratios and oscillation frequencies of the critical oscillation modes when there are no damping controllers in the system.

Modal analysis shows that without the damping controllers, the system is unstable for all three critical operating scenarios. There are three critical/unstable electromechanical modes including two poorly damped (damping ratio below 20%) local modes and an unstable interarea mode. The interarea mode has the poorest damping ratio in operating

Initialization of the population Xi ($i = 1, 2, \ldots, n$)
Initialization of GWO-PSO parameters, i.e., (a, A, C, w)
Calculation of fitness for each wolf in the population
The top three individual wolves with the highest fitness are recorded as $\overrightarrow{\mathbf{X}_\alpha}$, $\overrightarrow{\mathbf{X}_\beta}$ and $\overrightarrow{\mathbf{X}_\delta}$, respectively
While ($i <$ maximum iteration)
    For each wolf
        The position of the current individual is updated based on PSO using (29) and (30)
    End for
    The values for a, A, and C are updated
    The fitness value of all individuals is calculated
    $\overrightarrow{\mathbf{X}_\alpha}$, $\overrightarrow{\mathbf{X}_\beta}$ and $\overrightarrow{\mathbf{X}_\delta}$ is updated
    $i = i + 1$
End While
The position of the alpha wolf, $\overrightarrow{\mathbf{X}_\alpha}$, is returned

Algorithm 1: Pseudocode for the hybrid GWO-PSO.

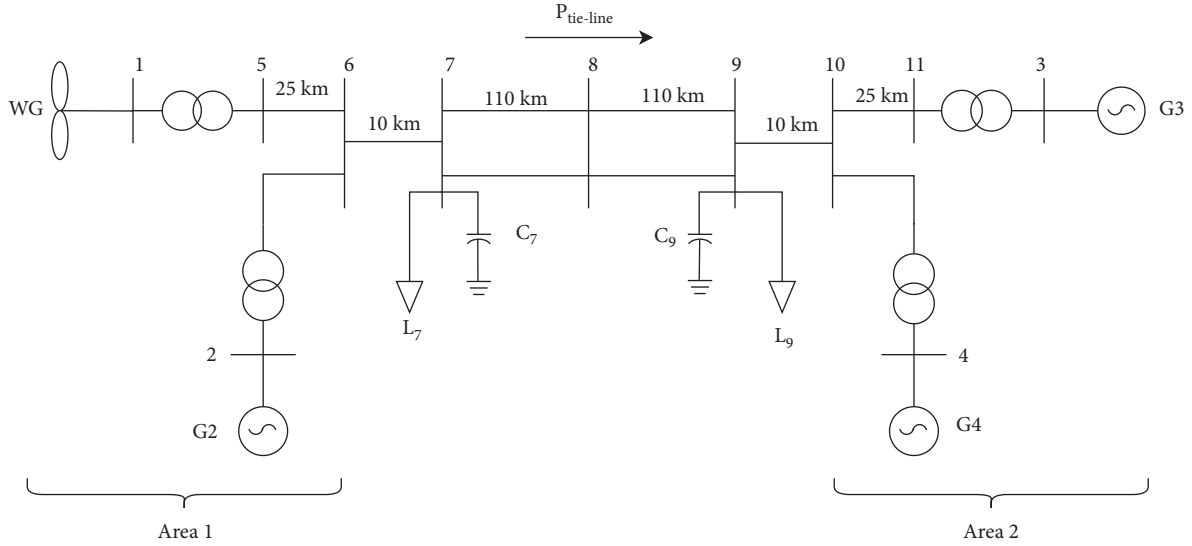

Figure 5: Single-line diagram for the 2A4G test system.

Table 1: System data and model assumptions.

Component	Parameters and/or model assumptions
Synchronous generators	Parameters are in per unit on base values of 900 MVA, 20 kV, and 60 Hz $X_d = 1.8$, $X_d' = 0.3$, $X_d'' = 0.25$, $X_q = 1.7$, $X_q' = 0.55$, $X_q'' = 0.25$, $R_a = 0.0025$, $T_{d0}' = 8$ s, $T_{d0}'' = 0.03$ s, $T_{q0}' = 0.4$ s, $T_{q0}'' = 0.05$ s, $A_{\text{sat}} = 0.015$, $B_{\text{sat}} = 9.6$, $\psi_{T1} = 0.9$, $H = 6.5$ s (for $G2$), $H = 6.175$ s (for $G3$ and $G4$), $K_D = 0$
Transmission lines	Parameters are in per unit on base values of 100 MVA and 20 kV. The line lengths are as shown in Figure 5. $r = 0.0001$ pu, $x_L = 0.001$ pu/km, $b_C = 0.00175$ pu/km
Transformers	Rating: 900 MVA, 20/230 kV$x = 0.15$ pu, off-nominal tap ratio = 1
Loads	Represented using static models with the active component modeled as constant current and the reactive components as constant impedance.
Excitor	$K_A = 200$, $T_R = 0.01$ s
PSS	The reference settings of the PSS are as follows:$K_{\text{STAB}} = 20$, $T_W = 10$ s, $T_1 = 0.05$ s, $T_2 = 0.02$ s, $T_3 = 3$ s, $T_4 = 5.4$ s
DFIG	Rating: 2 MVA, 0.69 kV. The DFIG parameters in per unit are as follows:$J = 75$ kgm^2, $R_S = 0.01$,$X_s = 0.1$,$X_m = 3.5$, $R_r = 0.01$, $X_r = 0.1$ The parameters for the DFIG control system are given in Ref. [23].The DFIG is connected to the main step-up transformer through a 0.69/20 kV transformer with $R = 0.001$ pu and $X = 0.06$ pu.

scenario 3 when the tie line power is the highest at 594 MW. At 4.05%, the wind farm mode ($M1$) is the least damped when the output of the DFIG is the highest at 700 MW. The local mode in Area 2 has the lowest damping ratio of 5.1% in the first operating scenario when the generators in that area have the highest loading. The oscillation frequencies for the

Table 2: Description of the critical operating scenarios.

Operating scenario no (MW)	1	2	3
DFIG power output	350	700	700
Generators $G2$, $G3$, and $G4$ active power output	750, 848, 850	700, 722, 700	700, 554, 700
Loads L_7, L_9 active power demand	967, 1767	967, 1767	767, 1767
Tie line power	118	398	594

local mode in Area 2 and the interarea mode are comparable to those of the benchmark two-area system [21]. At 2 Hz, the frequency for the DFIG mode is comparable to that of the 1.5 MW GE wind turbine-generator model with related model characteristics which is 1.8 Hz [34].

4.3. Modal Analysis with PSSs Only. The damping ratios and frequencies of the critical oscillation modes of the system when there are only PSSs in the system are shown in Table 4 below.

The system is stable unlike when there are no PSSs. The damping ratios of the local mode in area 2 and the interarea mode increase by a minimum of 16% and 20%, respectively, across the three critical operating scenarios. Although the local mode becomes sufficiently damped, the interarea mode is still poorly damped with the damping ratio being below 20% in all three critical operating scenarios. The improvement in the damping ratio of the two modes only comes at a cost of a slight increase in frequency by a maximum of 18.3% for the local mode and 8.8% for the interarea mode. The addition of the PSSs does not affect the DFIG mode, and the DFIG mode still has a maximum damping ratio of 4.64% among the three operating scenarios.

4.4. Modal Analysis considering Uncoordinated DFIG POD and PSSs. Before the optimization of the DFIG POD, the input signals for the POD need to be identified first. Eigenvalue analysis is carried out to find out the participation factors of the candidate feedback signals for the POD in the concerning modes. The feedback signal with the highest positive real participation factors is the most suitable input signal for the POD. The potential feedback variables ranked in terms of their participation in the critical modes are shown in Table 5.

From the analysis, as expected, the candidate local feedback variables for the POD have greater participation in the DFIG mode than in other critical modes. They have low participation in the interarea mode and the least participation in the local mode in Area 2. This confirms the observation that state variables associated with DFIG have minimal direct participation in other electromechanical modes of the system [11]. However, DFIG can indirectly influence the damping of other electromechanical modes through modulation of the power output of the DFIG. The shaft position (ϕ_{shaft}) state variable is determined to have the highest participation in the local wind farm mode. Thus, it has the most significant impact on the damping of the local DFIG mode, and potentially, the highest influence on other electromechanical modes of the system.

The shaft position is an integral part of the rotor speed deviation, which is the difference between the turbine speed and the generator speed. The proposed POD, therefore, considers the speed deviation as input which is a more practicable input with an equally high participation factor and is described as follows:

$$\Delta\omega = \frac{d\phi_{\text{shaft}}}{d\text{t}} = w_t - w_g. \tag{31}$$

The hybrid GWO-PSO algorithm explained in Section 3.3 is applied for the tuning of the DFIG POD, whose model is shown in Figure 3 The dimensionality of the optimization problem is five, taking into account the POD gain and four lead-lag phase compensation time constants. The optimal parameters for the POD are shown in Table 6. The PSSs, which are based on the model shown in Figure 1, retain the classical settings adapted from the benchmark system [21]. Both the POD and the PSSs have a washout time constant of 10 s, as mentioned in Section 2.1.

The damping ratios and frequencies of the critical oscillation modes with the uncoordinated design of the POD are shown in Table 7.

The uncoordinated DFIG POD suppresses the electromechanical oscillations in the wind farm. The damping ratio of the DFIG mode improves to above 20% in all the critical operating scenarios, with a decrease in oscillation frequency by a maximum of 14.8%. However, with a maximum damping ratio of 19.07%, the interarea mode is still poorly damped in all the critical operating scenarios.

4.5. Modal Analysis with the Proposed Robust Coordinated Design of POD and PSSs. The simultaneous robust coordinated strategy in the design of several damping controllers is implemented in the study system. The proposed optimization technique applying hybrid GWO-PSO is employed to search for the optimal values for damping controllers' parameters. The DFIG POD utilizes the rotor speed deviation which is identified as the most effective feedback signal in Section 4.4. The operating scenarios outlined in Table 2 are applied to ensure that the optimized damping controllers are robust enough to cope with the critical operating scenarios of the study system.

The optimization problem has a dimensionality of 20 comprising five parameters for each of the four damping controllers in the study system. The damping controllers are tuned through peer-to-peer communication between DIgSILENT PowerFactory and MATLAB, considering the constraints in Section 3.2. The optimized parameters of the damping controllers are outlined in Table 8.

Table 9 below shows the damping ratios and frequencies of the critical oscillation modes of the system with the

Table 3: Critical oscillatory modes without damping controllers.

Operating scenario	Mode	Eigenvalue	Frequency (Hz)	Damping ratio (%)	Participating generators
1	M1	$-0.5920 \pm j12.7266$	2.025	4.64	*WG*
	M2	$-0.3767 \pm j7.3648$	1.172	5.10	*G*3, *G*4
	M3	$0.1253 \pm j4.7558$	0.757	−2.63	All *G*
2	M1	$-0.5167 \pm j12.7364$	2.027	4.05	*WG*
	M2	$-0.6908 \pm j7.1551$	1.139	9.61	G3, G4
	M3	$0.2046 \pm j4.1643$	0.663	−4.91	All G
3	M1	$-0.5163 \pm j12.7357$	2.027	4.05	WG
	M2	$-0.8743 \pm j6.9612$	1.108	12.46	*G*3, *G*4
	M3	$0.3087 \pm j2.9894$	0.476	−10.27	All *G*

Table 4: Critical oscillation modes considering the PSSs only.

Operating scenario	Mode	Eigenvalue	Frequency (Hz)	Damping ratio (%)	Participating generators
1	*M*1	$-0.5917 \pm j12.7268$	2.026	4.64	*WG*
	*M*2	$-1.9960 \pm j8.7160$	1.387	22.32	*G*3, *G*4
	*M*3	$-0.9419 \pm j4.8489$	0.772	19.07	All *G*
2	*M*1	$-0.5165 \pm j12.7373$	2.027	4.05	*WG*
	*M*2	$-2.2823 \pm j8.3930$	1.336	26.24	*G*3, *G*4
	*M*3	$-0.6929 \pm j4.2338$	0.674	16.15	All *G*
3	*M*1	$-0.5162 \pm j12.7368$	2.027	4.05	*WG*
	*M*2	$-2.3802 \pm j7.9815$	1.270	28.58	*G*3, *G*4
	*M*3	$-0.3196 \pm j3.2528$	0.518	9.77	All *G*

Table 5: Modal participation factors for potential POD feedback signals.

Candidate feedback variable	Local wind farm mode	Local mode, area 2	Interarea mode
ϕ_{shaft}	1.00000	0.00000	0.00011
ω_t	0.88058	0.00000	0.00000
ω_g	0.12916	0.00000	0.00012
P_{ref}	0.01300	0.00000	0.00004
$i_{d\text{ref}}$	0.00276	0.00002	0.00473

Table 6: Parameters of damping controllers with uncoordinated optimization.

Damping controller	K	T_1	T_2	T_3	T_4
*G*2, *G*3, *G*4 PSSs	20	0.05	0.02	3	5.4
DFIG POD	0.2	1	1	0.1	0.1

Table 7: The oscillation modes with uncoordinated design of POD.

Operating scenario	Mode	Eigenvalue	Frequency (Hz)	Damping ratio (%)	Participating generators
1	*M*1	$-2.3476 \pm j10.8467$	1.726	21.15	*WG*
	*M*2	$-1.9961 \pm j8.7160$	1.387	22.32	*G*3, *G*4
	*M*3	$-0.9418 \pm j4.8491$	0.772	19.07	All *G*
2	*M*1	$-2.3200 \pm j11.0844$	1.764	20.49	*WG*
	*M*2	$-2.2822 \pm j8.3929$	1.336	26.24	*G*3, *G*4
	*M*3	$-0.6928 \pm j4.2339$	0.674	16.15	All *G*
3	*M*1	$-2.3543 \pm j11.0934$	1.766	21.15	*WG*
	*M*2	$-2.3803 \pm j7.9814$	1.270	28.58	*G*3, *G*4
	*M*3	$-0.3196 \pm j3.2529$	0.518	9.78	All *G*

proposed robust coordinated strategy in the design of the damping controllers.

The damping ratios of all the critical oscillation modes are improved to above 20% across the three critical operating scenarios in contrast to the case of uncoordinated POD and PSSs. While the coordination only improves the damping ratio of the DFIG mode (*M*1) by less than 1%, the damping ratio of the local mode in Area 2 (*M*2) and the interarea

Table 8: Parameters of damping controllers with coordinated optimization.

Damping controller	K	T_1	T_2	T_3	T_4
DFIG POD	0.20	0.97	0.10	1.00	0.10
G2 PSS	35.22	0.01	0.01	0.01	0.08
G3 PSS	18.67	0.01	0.06	0.15	0.10
G4 PSS	47.93	0.04	0.01	0.01	0.01

mode ($M3$) increases by a minimum of 9.4% and 50.7%, respectively. While the coordination barely affects the frequency of the DFIG mode, the frequency of the local mode increases by a maximum of 33.8%, while that of the interarea mode reduces by a maximum of 43.3%.

In summary, the findings of this study are summarized as follows:

(1) The absence of controllers in the system makes the interarea mode unstable, while the DFIG mode and the local mode in area 2, both with a damping ratio below 20%, are poorly damped in all three critical operating scenarios.

(2) The inclusion of PSSs only in the system stabilizes the interarea mode. The PSSs do not affect the DFIG mode. The PSSs improve the damping ratios of the local mode in Area 2 and the interarea mode by a minimum of 16% and 20%, respectively, across the three critical operating scenarios.

(3) The introduction of the POD, in addition to the PSSs, improves the damping ratio of the DFIG mode by a minimum of 16.5% without directly affecting the other critical modes. The DFIG mode becomes sufficiently damped in all the critical operating scenarios.

(4) The coordination of the POD and the PSSs using the proposed strategy further increases the damping ratio of the local mode in Area 2 and the interarea mode by a minimum of 9.4% and 50.7%, respectively, while only increasing the damping ratio of the DFIG mode by an average 0.4%. All the dominant modes in the system are sufficiently damped with a damping ratio above 20% in all three critical operating scenarios.

The proposed method achieves comparable results to other related methods investigated in literature. For the most closely related operating condition, the coordination of only DFIG POD and PSSs in this study achieves better performance in the damping of interarea oscillations mode when compared with the study in Ref. [18], where DFIG POD, SVC POD, and PSSs were coordinated. The global mode in which DFIG and the synchronous generators participate ($M3$ in this study) had a damping ratio of 57.1% compared to 60.45% (Table 9), even with extra tie line power of 12 MW. The performance improvement could be attributed to the less synchronous generators in this study, the use of a large-scale wind farm (700 MW), the selection of local rotor speed deviation as the input for the DFIG POD, and the application of hybrid GWO-PSO for optimization.

Mehta et al. [35] agreed with the results in this study that the substitution of a $G1$ with a WECS of equal capacity in the two-area system without damping controllers results in instability of the interarea mode. Furthermore, for the most comparable operating scenario 2, the damping ratio of the interarea mode in this study agrees with the results obtained in their work, considering only PSSs. While the authors obtained an interarea mode with a damping ratio of 13.34%, a damping ratio of 16.15% was obtained in this study as shown in Table 4. The difference in damping ratio could be occasioned by slightly different settings for the excitation system, the DFIG control system, and the PSSs.

The use of a combination of POD and PSSs, which are installed in large-scale wind farm (700 MW) and synchronous generators, respectively, has a substantial improvement in the damping ratios of the critical modes compared with only decentralized PODs used with medium-scale wind farms (100 MW) in Ref. [17]. While the coordination of the two decentralized PODs only results in a minimum improvement of 4.7% in the damping ratio of the critical modes, the coordination of POD and PSSs in this study results in a minimum improvement of 17.1%.Whereas the consideration of additional damping controllers in this study could be the key contribution to the improvement, other factors such as the use of GWO-PSO in contrast to the firefly algorithm used in their study could also play part in the improvement.

4.6. Testing the Robustness of the Coordinated Strategy. It is desired that the proposed coordinated design method ensures that the damping controllers in the system consistently ensure that electromechanical oscillations in the system are sufficiently damped regardless of the state of the power system at any given time. The power system is a complex system with diverse operating states. The presence of DFIG, which runs on intermittent wind resource, further increases the number of operating conditions in the system.Although the damping controllers are designed considering some of the worst-case operating conditions with regard to small-signal stability, it is paramount to ensure that the damping controllers are robust enough to handle most of the operating conditions that are present.

Monte Carlo simulation is used to generate 1000 sample operating conditions to investigate the robustness of the coordinated design strategy. The simulation of the operating scenarios is implemented in MATLAB. Each operating scenario considers different active power outputs for the DFIG and the synchronous generators,

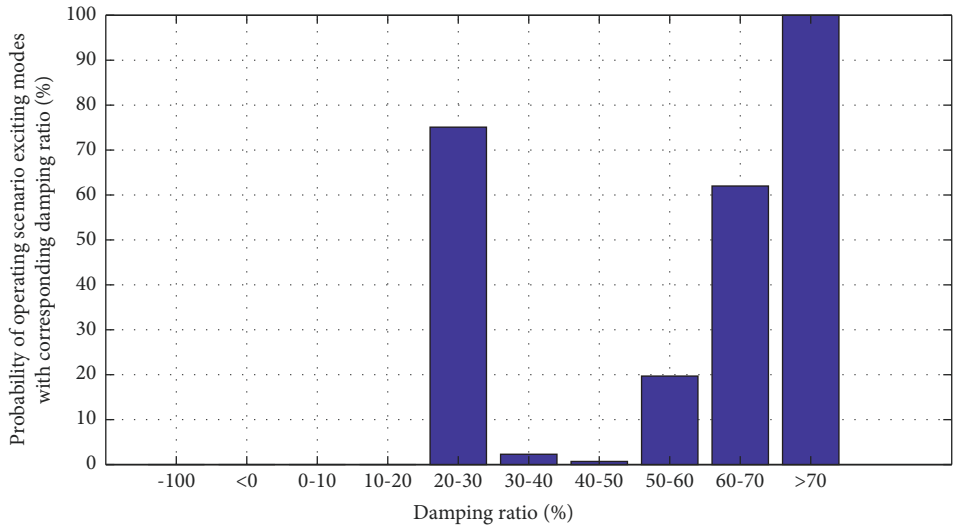

Figure 6: Probability of operating scenarios exciting modes whose damping ratio is within particular bounds.

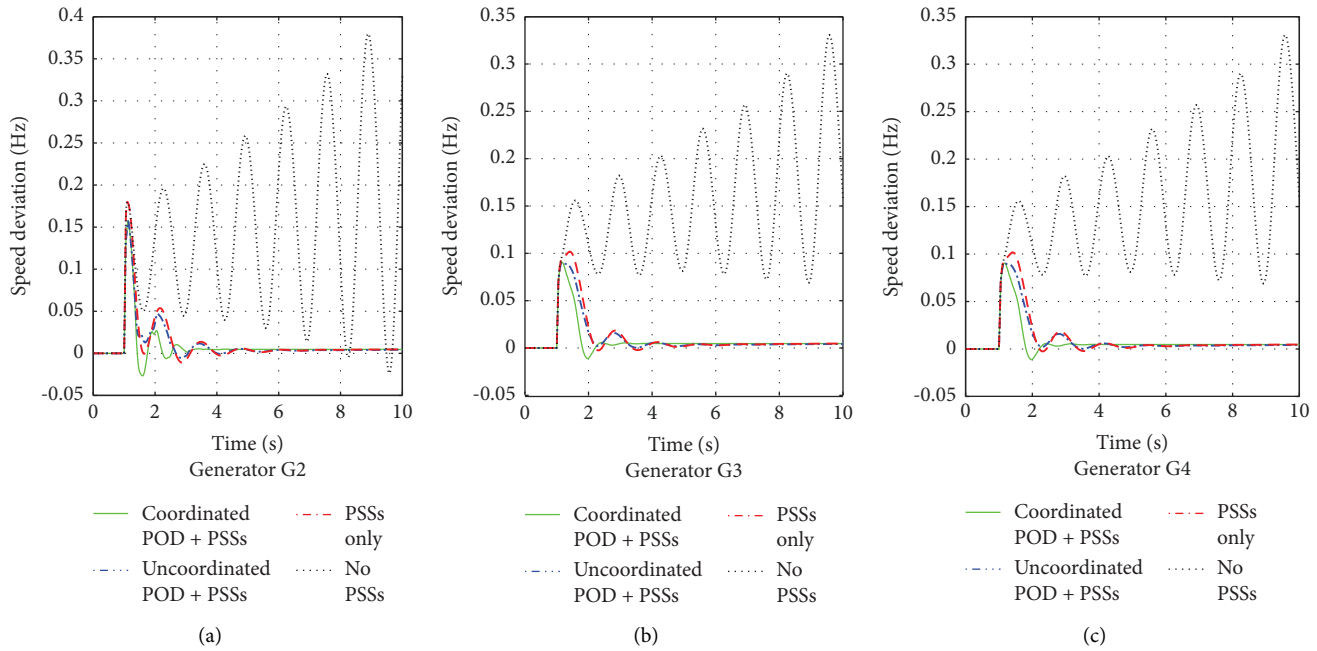

Figure 7: Synchronous generators' speed deviation responses to a three-phase fault in line 7-8 in the critical operating scenario 1.

different active and reactive power demands for the loads, and different outage scenarios for lines 7-8 in Figure 5. The DFIG output is simulated based on the Weibull probability distribution, with a scale factor of 1.23 and a shape factor of 1.75, generated from DIgSILENT PowerFactory wind characteristic [23]. A minimum limit of 175 MW was imposed on the DFIG output to satisfy power flow constraints. The active power of the generators is simulated using a uniform probability distribution. The generator power output is allowed to vary between ± 20% of the rated output. The active power of the loads is also simulated using a uniform probability distribution. The load is allowed vary to not less than 20% of the rated demand. The corresponding reactive power of the load is calculated such that a uniform power factor is maintained. The line outage is simulated based on binomial probability distribution, where the probability of a line outage in each operating scenario is 10%.

Each of the simulated operating scenarios is transferred from MATLAB to DIgSILENT PowerFactory through a communication interface, and the corresponding eigenvalues are used to determine the probability that a particular operating scenario will excite modes whose damping ratio is within particular bounds. Figure 6

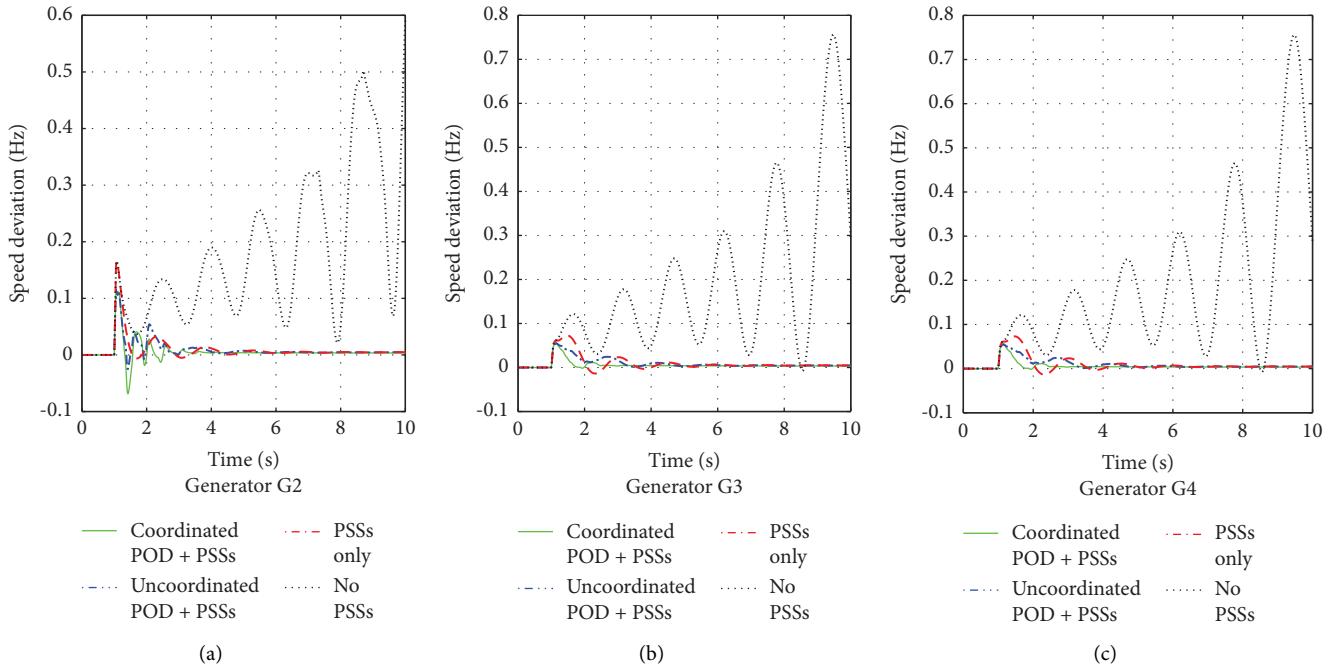

Figure 8: Synchronous generators' speed deviation responses to a three-phase fault in line 7-8 in the critical operating scenario 2.

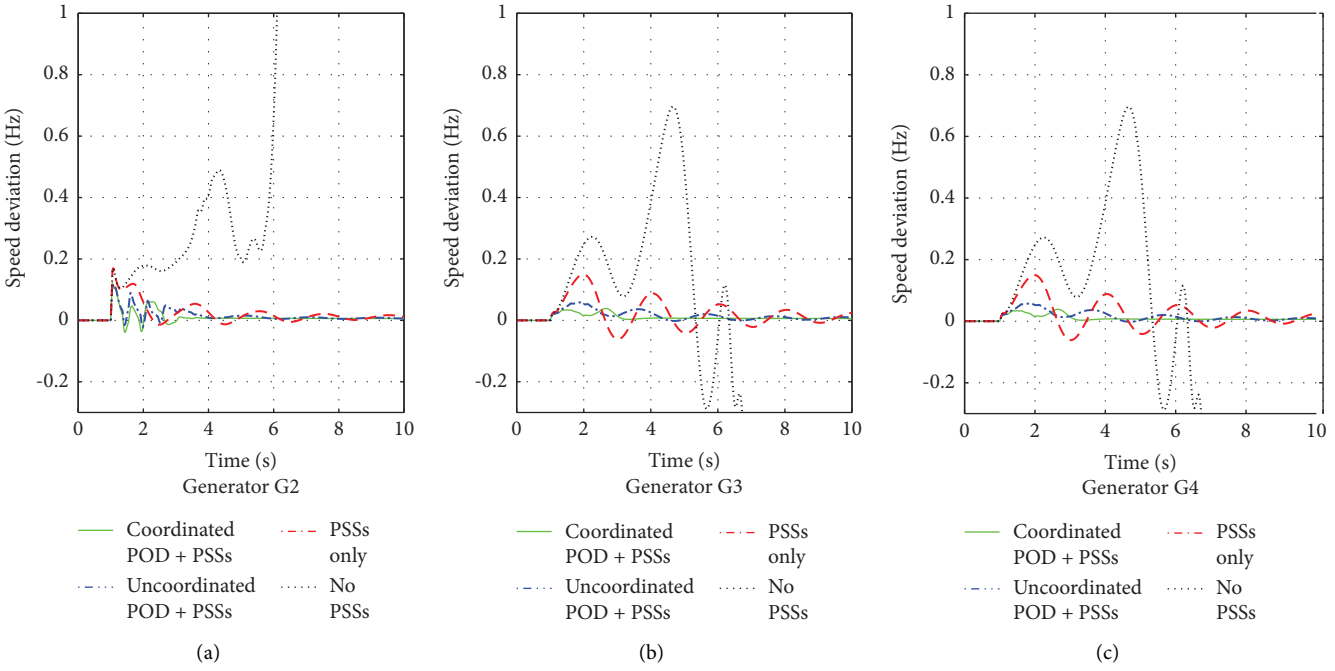

Figure 9: Synchronous generators' speed deviation response to a three-phase fault in line 7-8 in the critical operating scenario 3.

depicts the findings of the probability analysis. It is observed that there is no probability of any particular operating scenario exciting modes which have a damping ratio below 20%. Therefore, the coordinated damping controllers are robust enough to handle any operating condition provided the power flow and system control constraints are met.

4.7. Nonlinear Time-Domain Simulation. Nonlinear time-domain simulations are performed to further verify the damping performance of the robust coordinated design strategy. The simulations are conducted for the four aforementioned damping controller cases and the three critical operating scenarios where the respective dominant modes have the poorest damping. A three-phase self-

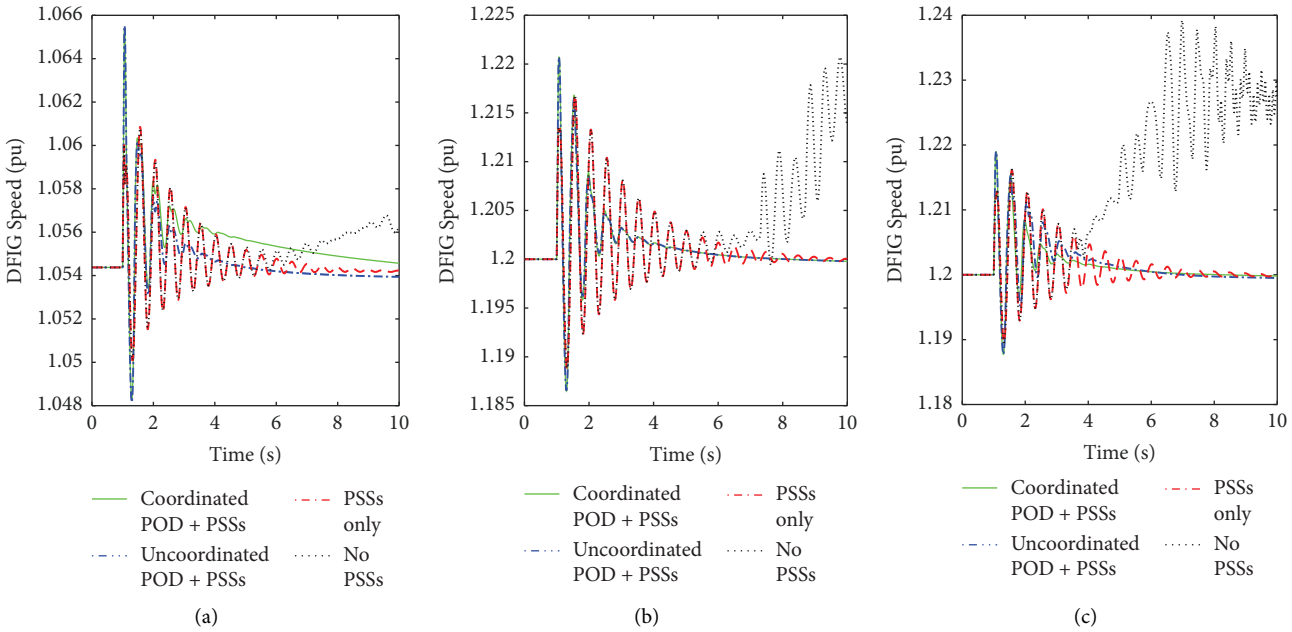

Figure 10: DFIG speed response to a three-phase fault in line 7-8 under different critical operating scenarios: (a) Operating scenario 1; (b) operating scenario 2; (c) operating scenario 3.

Table 9: The oscillation modes with the coordinated design of POD and PSSs.

Operating scenario	Mode	Eigenvalue	Frequency (Hz)	Damping ratio (%)	Participating generators
1	$M1$	$-2.3677 \pm j10.9968$	1.750	21.05	WG
	$M2$	$-4.1695 \pm j11.5795$	1.843	33.88	$G3$, $G4$
	$M3$	$-4.2083 \pm j2.7386$	0.438	83.8	All G
2	$M1$	$-2.4521 \pm j11.2703$	1.794	21.26	WG
	$M2$	$-4.2521 \pm j11.1357$	1.772	35.66	$G3$, $G4$
	$M3$	$-3.6147 \pm j3.6181$	0.576	70.68	All G
3	$M1$	$-2.5035 \pm j11.2761$	1.795	21.67	WG
	$M2$	$-4.6042 \pm j10.6739$	1.699	39.61	$G3$, $G4$
	$M3$	$-2.7855 \pm j3.6703$	0.584	60.45	All G

clearing fault is considered at 50% of one of the tie line between bus 7 and bus 8 in Figure 5. It is assumed that the fault clears after 3 cycles (50 ms).

The speed deviation of the synchronous generators with respect to the reference bus, in the critical operating scenarios 1, 2, and 3 are shown in Figures 7–9, respectively. The DFIG speed in the three critical operating scenarios is shown in Figure 10.

It is observed that without damping controllers, the synchronous machines in the system lose synchronism after the fault is cleared in all the critical operating scenarios. The oscillations in the DFIG speed grow, which is undesirable. The rest of the three cases, where a damping controller is present, results in the oscillations being damped, albeit at different levels. When only the PSSs are present in the system, the oscillations exhibit higher overshoot and settling times than the other cases where the POD is present. In the case of uncoordinated POD and PSSs, where the PSSs use classical settings and DFIG is optimized separately, it is observed that the DFIG POD brings along a significant contribution in the damping of oscillations compared with when only PSSs are present in the system. With the DFIG POD, the oscillations in the DFIG speed and those in the generator speed deviation have considerably lower overshoot and lower settling time compared to only when PSSs are present.

The coordination of the POD and the PSSs in the system has the most superior damping performance, judging by the overshoot and settling time, among the four cases. It not only outperforms the uncoordinated damping control in suppressing the overshoot of the oscillations but also achieves a shorter settling time. This means the steady-state operation state of the system is achieved faster after the fault is cleared when the damping controllers are coordinated. In the coordinated design strategy, the DFIG POD optimizes the interactions between the DFIG and the other synchronous generators ensuring superior damping of not only the local modes but also the global modes. The consistent effective performance of the coordinated design strategy under the different critical operating scenarios proves its robustness in

damping oscillations. Since the coordinated POD and PSSs perform effectively in these worst-case operating scenarios, it is expected that they perform well under all other operating scenarios, provided the system power flow and control constraints are met.

The time-domain simulations results agree with the results for the eigenvalue and the probabilistic Monte Carlo analyses that the coordinated strategy not only provides the most superior damping performance among the four controller cases investigated but is also the most robust.

5. Conclusion

The theoretical feasibility and capability of coordinating several kinds of damping controllers in a power system, including PSSs and DFIG POD, in a multimachine power system with a large-scale WECS are investigated in this work. The optimization of the parameters of the PSSs and the POD is carried out concurrently. The modal participation factor is used to identify the most effective DFIG-based feedback signal for the POD. A robust multiobjective eigenvalue-based value approach is formulated to facilitate the optimization of the damping controllers' parameters. The recent hybrid GWO-PSO is applied to search for the most ideal parameters for the PSSs and the POD. Linear modal analysis is used to establish the theoretical feasibility and the potency of the proposed coordinated strategy in the design of multiple damping controllers using a modified two-area four-generator benchmark system. Nonlinear time-domain simulations are used to verify the results of the linear eigenvalue analysis. The coordinated damping approach is found to be far more effective in damping network oscillations than when only one type of damping controller, the PSS, is used. What is more, the coordinated strategy outperformed the uncoordinated design not merely in damping local oscillations modes but also in damping interarea modes. Through the implementation of the coordinated design strategy, the DFIG can coordinate with other synchronous generators in suppressing low-frequency oscillations and improving the dynamic stability of the power system. The feasibility and superior performance of the coordinated design of multiple damping controllers in a power system with large-scale WECS are thus demonstrated.

It should be kept in mind that the coordinated design strategy that is proposed in this work can be scaled to other multiple kinds of damping controllers including controllers for flexible AC transmission systems (FACTS) to enhance not just power system dynamic performance but also voltage support. However, how to use the proposed strategy for large power systems involving many controllers is still ongoing research. The proposed strategy considers only critical operating scenarios to ensure the robust performance of the coordinated design strategy while reducing the computational burden. To consider more operating scenarios to further enhance robustness, the application of parallel computing and intelligent algorithms capable of handling higher dimensional optimization problems should be explored for large power systems. While the critical operating scenarios might be sufficient to achieve robustness, other operating scenarios occasioned by the stochastic uncertainty of WECS due to ungovernable wind speeds should be considered in the future work.

Data Availability

The data used to support the findings of this study are available from the corresponding author upon request.

Conflicts of Interest

The authors declare that they have no conflicts of interest.

Acknowledgments

This work was funded by the African Union Research Grant.

References

[1] W. Wang, L. Wu, H. Xu, W. Liu, and X. Chen, "A study of novel power system stabilizer," *IFAC Proceedings Volumes*, vol. 36, no. 20, pp. 1047–1050, 2003.

[2] R. Cardenas, R. Pena, S. Alepuz, and G. Asher, "Overview of control systems for the operation of DFIGs in wind energy applications," *IEEE Transactions on Industrial Electronics*, vol. 60, no. 7, pp. 2776–2798, 2013.

[3] J. Pollefliet, *15 - Applications of Power Electronics*, J. B. T.-P. E. Pollefliet, Ed., 15.44 pages, Academic Press, China, 2018.

[4] H. Holttinen, J. Kiviluoma, D. Flynn et al., "System impact studies for near 100% renewable energy systems dominated by inverter based variable generation," *IEEE Transactions on Power Systems*, vol. 37, no. 4, pp. 3249–3258, 2022.

[5] D. Flynn, Z. Rather, A. Ardal et al., "Technical impacts of high penetration levels of wind power on power system stability," *WIREs Energy and Environment*, vol. 6, no. 2, 2017.

[6] A. Rashad, S. Kamel, and F. Jurado, *The Basic Principles of Wind Farms*, Elsevier, Tharamani, Chennai, 2017.

[7] E. L. Miotto, P. B. De Araujo, E. De Vargas Fortes, B. R. Gamino, and L. F. B. Martins, "Coordinated tuning of the parameters of PSS and POD controllers using bioinspired algorithms," *IEEE Transactions on Industry Applications*, vol. 54, no. 4, pp. 3845–3857, 2018.

[8] Y. Xing, B. Marinescu, M. Belhocine, and H. Chen, "Power Oscillations Damping Controller for HVDC Inserted in Meshed AC Grids to Cite This Version," *HAL Id : Hal-02512398 Power Oscillations Damping Controller for HVDC Inserted in Meshed AC Grids*, Beijing, 2020.

[9] M. E. Aboul-Ela, A. A. Sallam, J. D. McCalley, and A. A. Fouad, "Damping controller design for power system oscillations using global signals," *IEEE Transactions on Power Systems*, vol. 11, no. 2, pp. 767–773, 1996.

[10] F. Dussaud, *An Application of Modal Analysis in Electric Power Systems to Study Inter-area Oscillations*, p. 87, NY China, 2015.

[11] Â. Mendonça and J. A. Peças Lopes, "Robust tuning of power system stabilisers to install in wind energy conversion systems," *IET Renewable Power Generation*, vol. 3, no. 4, pp. 465–475, 2009.

[12] O. Anaya-Lara, *Power System Stabiliser for a Generic DFIG-Based Wind Turbine Controller*, pp. 145–149, China, 2006.

[13] T. Surinkaew and I. Ngamroo, "Robust power oscillation damper design for DFIG-based wind turbine based on

specified structure mixed H2/H∞ control," *Renewable Energy*, vol. 66, pp. 15–24, 2014.

[14] K. Elkington, M. Ghandhari, L. Soder, and L. Söder, "Using Power System Stabilisers in Doubly Fed Induction Generators," in *Proceedings of the 2008 Australasian Universities Power Engineering Conference*, pp. 1–6, Kurukshetra, India, December 2008.

[15] K. Thanpisit and I. Ngamroo, "Power oscillation damping control by PSS and DFIG wind turbine under multiple operating conditions," *Turkish Journal of Electrical Engineering and Computer Sciences*, vol. 25, no. 5, pp. 4354–4368, 2017.

[16] H. Huang and C. Y. Chung, "Coordinated damping control design for DFIG-based wind generation considering power output variation," *IEEE Transactions on Power Systems*, vol. 27, no. 4, pp. 1916–1925, 2012.

[17] T. Surinkaew and I. Ngamroo, "Power system oscillations damping by robust decentralized DFIG wind turbines," *Journal of Electrical Engineering and Technology*, vol. 10, no. 2, pp. 487–495, 2015.

[18] J. Zuo, Y. Li, D. Shi, and X. Duan, "Simultaneous robust coordinated damping control of power system stabilizers (PSSS), static var compensator (SVC) and doubly-fed induction generator power oscillation dampers (DFIG PODs) in multimachine power systems," *Energies*, vol. 10, no. 4, p. 565, 2017.

[19] M. A. M. Shaheen, H. M. Hasanien, and A. Alkuhayli, "A novel hybrid GWO-PSO optimization technique for optimal reactive power dispatch problem solution," *Ain Shams Engineering Journal*, vol. 12, no. 1, pp. 621–630, 2021.

[20] S. Essallah, A. Bouallegue, and A. Khedher, "Integration of automatic voltage regulator and power system stabilizer: small-signal stability in DFIG-based wind farms," *J. Mod. Power Syst. Clean Energy*, vol. 7, no. 5, pp. 1115–1128, 2019.

[21] P. Kundur, N. J. Balu, and M. G. Lauby, *Power System Stability and Control*, McGraw-Hill, New York, 1994.

[22] J. T. Jose and C. A. Baran, "Performance analysis of doubly fed induction generator - a magnetic saturation perspective," *Int. J. Circuits, Syst. Signal Process.*vol. 13, pp. 563–569, 2019.

[23] DIgSILENT GmbH, *PowerFactory 2021 Brochure*pp. 1–28, Beijing, 2021.

[24] L. Fan, H. Yin, and Z. Miao, "On active/reactive power modulation of DFIG-based wind generation for interarea oscillation damping," *IEEE Transactions on Energy Conversion*, vol. 26, no. 2, pp. 513–521, 2011.

[25] A. G. Phadke and J. S. Thorp, *Phasor Measurement Units and Phasor Data Concentrators BT - Synchronized Phasor Measurements and Their Applications*, A. G. Phadke and J. S. Thorp, Eds., Springer International Publishing, Cham, pp. 83–109, 2017.

[26] A. Stativa, M. Gavrilas, and V. Stahie, "Optimal tuning and placement of power system stabilizer using particle swarm optimization algorithm," in *Proceedings of the 2012 International Conference and Exposition on Electrical and Power Engineering*, pp. 242–247, Beijing China, June 2012.

[27] S. Mirjalili, S. M. Mirjalili, and A. Lewis, "Grey wolf optimizer," *Advances in Engineering Software*, vol. 69, pp. 46–61, 2014.

[28] N. Singh and S. B. Singh, "Hybrid algorithm of particle swarm optimization and grey wolf optimizer for improving convergence performance," *Journal of Applied Mathematics*, vol. 2017, pp. 1–15, Article ID 2030489, 2017.

[29] J. Kennedy and R. Eberhart, "Particle swarm optimization," *Proceedings of ICNN'95 - International Conference on Neural Networks*, vol. 4, p. 1942, 1995.

[30] N. Nahak and R. K. Mallick, "Enhancement of small signal stability of power system using UPFC based damping controller with novel optimized fuzzy PID controller," *Journal of Intelligent and Fuzzy Systems*, vol. 35, no. 1, pp. 501–512, 2018.

[31] M. Manohar, E. Koley, and S. Ghosh, "Investigation and damping of low frequency oscillations of stochastic solar penetrated power system by optimal dual UPFC controller," *IET Science, Measurement & Technology*, vol. 45, no. 2–13, 2018.

[32] M. J. Islam, M. S. R. Tanveer, and M. A. H. Akhand, "A comparative study on prominent nature inspired algorithms for function optimization," in *Proceedings of the 2016 5th 2016 5th International Conference on Informatics, Electronics and Vision (ICIEV)*, pp. 803–808, Seoul Korea, June 2016.

[33] M. Klein, G. J. Rogers, and P. Kundur, "A fundamental study of inter-area oscillations in power systems," *IEEE Transactions on Power Systems*, vol. 6, no. 3, pp. 914–921, 1991.

[34] K. Clark, N. W. Miller, and J. J. Sanchez-gasca, *Modeling of GE Wind Turbine-Generators for Grid Studies*, Cham, 2008.

[35] B. Mehta, P. Bhatt, and V. Pandya, "Small signal stability analysis of power systems with DFIG based wind power penetration," *International Journal of Electrical Power & Energy Systems*, vol. 58, pp. 64–74, 2014.